N-153, 142

NASA TECHNICAL MEMORANDUM

NASA TM-76930

COMPUTATION OF SUBSONIC FLOW AROUND AIRFOIL SYSTEMS WITH MULTIPLE SEPARATION

Klaus Jacob

Translation of "Berechnung von Profilsystemen bei Unterschallstromung mit mehrfacher Ablosung). DFVLR, Institut fuer Theoretische Stromungsmechanik, Goettingen, West Germany, DFVLR-FB-81-24, 1981, 63p.

NATIONAL AERONAUTICS AND SPACE ADMINISTRATION
WASHINGTON, D. C. 20546 JUNE 1982

STANDARD TITLE PAGE

1. Report No. NASA TM-76930	2. Government Accession No.	3. Recipient's Catalog No.
4. Title and Subtitle COMPUTATION OF SUBSONIC FLOW AROUND AIRFOIL SYSTEMS WITH MULTIPLE SEPARATION		5. Report Date JUNE 1982
		6. Performing Organization Code
7. Author(s) Klaus Jacob		8. Performing Organization Report No.
		10. Work Unit No.
9. Performing Organization Name and Address SCITRAN Box 5456 Santa Barbara, CA 93108		11. Contract or Grant No. NASw- 3542
		13. Type of Report and Period Covered Translation
12. Sponsoring Agency Name and Address National Aeronautics and Space Administration Washington, D.C. 20546		14. Sponsoring Agency Code

15. Supplementary Notes

Translation of "Berechnung von Profilsystemen bei unterschallstromung mit mehrfacher Ablosung)". DFVLR, Institut fuer Theoretische Stromungsmechanik, Goettingen, West Germany, DFVLR-FB-81-24, 1981, 63 p. (N82-14050)

16. Abstract

A numerical method for computing the subsonic flow around multi-element airfoil systems has been developed, allowing for flow separation at one or more elements. Besides multiple rear separation also short bubbles on the upper surface and cove bubbles can approximately be taken into account. Also, compressibility effects for pure subsonic flow are approximately accounted for. After presentation the method is applied to several examples and improved in some details. Finally, the present limitations and desirable extensions are discussed.

17. Key Words (Selected by Author(s))	18. Distribution Statement Unclassified - Unlimited

19. Security Classif. (of this report) Unclassified	20. Security Classif. (of this page) Unclassified	21. No. of Pages 61	22. Price

TABLE OF CONTENTS

COMPUTATION OF SUBSONIC FLOW AROUND AIRFOIL SYSTEMS WITH MULTIPLE SEPARATION*

Klaus Jacob**

SUMMARY

A numerical method for computing the subsonic flow around multi-element airfoil systems has been developed, allowing for flow separation at one or more elements. Besides multiple rear separation also short bubbles on the upper surface and cove bubbles can approximately be taken into account. Also, compressibility effects for pure subsonic flow are approximately accounted for. After presentation the method is applied to several examples and improved in some details. Finally, the present limitations and desirable extensions are discussed.

NOTATION ***/6

a_1, a_2	superposition factors for the corresponding basic solutions (a_1), (a_2)
$A_{i,m}$	m-th connection point for the dead water on profile number i
b_i	superposition factor for basic solution (b_i), i.e., pure circulation flow around profile number i
c_a	lift coefficient
c_p	pressure coefficient $= (p - p_\infty)/(V_\infty^2 \rho/2)$
$c_{m1/4}$	pitch moment coefficient, referred to the 1/4 point
$d_{i,m}$	superposition factor for the basic solution $(d_{i,m})$, i.e., pure outflow from profile number i, where the source occupation starts at point $A_{i,m}$
E	yield of source occupation
H	trailing edge

* DFVLR Research Report 81-24, 1981, 63 pages.

** Institute for Theoretical Fluid Mechanics of DFVLR, Goettingen.

*** Numbers in margin indicate pagination of foreign text.

$K(\varphi,\psi)$ $L(\varphi,\psi)$	geometric functions defined by equation (2d) and equation (2e)
l	profile chord
Ma_∞	Mach number of incident flow
M_k	number of given support point on the contour of profile number k
N	number of profiles in the profile system
O_i	point on the upper boundary line of the dead water region of profile i
p, p_∞	static pressure and static pressure of incident flow respectively
Re	Reynolds number = $V_\infty \cdot l$ kinematic viscosity
s	running length along profile contour or gap distance (in Figure 13)
t	various lengths in Figures 4 and 13
U_i	attachment point of dead water region along the underside of profile i
v	local flow speed
v_∞	incident flow speed
V_∞	incident flow speed of resulting flow
v_n, v_t	normal and tangential component of flow speed along profile contour. These are identical with the intensity of a surface source and vortex occupation
v_x, v_y	x and y components of flow speed
x, y	cartesian coordinates
α	angle of attack
δ_1, δ_2	displacement thickness and momentum loss thickness of boundary layer
ϕ_k, ψ_j	parameters; to each value of for example ϕ_k there is the unique contour point of the profile number k associated with it
Γ_i	circulation around profile i
κ	adiabatic exponent
ω_n	transformed source intensity according to equation (2b)
ω_t	transformed vortex intensity according to equation (2a)
ρ	density of flowing medium

Subscripts:

i, j, k running numbers of profile

m, μ, ν running numbers of points on profile contours

∞ in the flow far away from the profile system

LA at the separation point of the laminar boundary layer

1. INTRODUCTION /9

Wings with slats and slot flaps (mechanical lift aids) have for a long time been used to improve the takeoff and landing performances of aircraft. The longitudinal section through such a wing system results in a profile system (see, for example Figure 14, top).

Over the last few decades intensive experimental and theoretical profile research has led to substantial improvement of individual profiles, for example, substantially reduced drag for fast flight due to the development of laminar profiles and over-critical profiles. There has also been improved high lift and stall behavior by suitable curvature, S-shape, etc. Improvements to the (two-dimensional) profiles have also resulted in better (three-dimensional) wings especially for large wing aspect ratios. The calculation possibilities for individual profiles have advanced considerably. For incompressible, frictionless flow, very exact surface singularity methods are available. Friction and even flow separation can be approximately considered in calculations.

On the other hand, for profile systems, the magnitude of available experimental data as well as the possibility of calculation are rather restricted. The high lift configurations which are very important for takeoff and landing of our aircraft have developed empirically for the most part. The calculation of such profile systems can be done for frictionless flow using singularity methods (see, for example, [1-3]), but friction and partial separation are even more important in practice than is the case for individual profiles. Calculation methods for profile systems with friction and separation are still in the beginning stages of development. The aircraft industry is very interested in reliable and practical calculation methods of this type in order to develop better high lift configurations for new aircraft and to reduce the experimental expenditure.

Based on the calculation method for the individual profile with flow separation [4] developed by the author, during the 70's several similar methods were developed for profile systems, for example, z. B. von BHATELEY and BRADLEY [5], JACOB and STEINBACH /10
[6], HAYASHI and ENDO [7] and OLSON [8]. All of these methods have one common feature in that a potential flow with an imbedded simulated dead water region is calculated using surface singularities and this is combined with boundary layer calculations using iterations. Differences between the individual methods occur in the modeling of the dead water region and in the boundary layer method used. All of the methods up to the present were restricted to analyzing pure trailing edge separation, and additional possible physical phenomena such as separation bubbles, bottom side separation, compressibility effect were not considered. Wake boundary layer confluence is only included approximately in [8]. A ground influence is only considered in [6,6b]. Most methods are restricted to simple separation, that is, separation at only one element of the profile system.

A general and really reliable calculation method can only be developed in steps by researching all of the possible physical phenomena, continuously comparing them with experiments, theoretical modeling and these all have to be included in the calculations. In addition, reliable criteria for the occurrence of individual phenomena are required. Of course, a restricted method can be useful but only if its limitations are known and it is appropriately applied.

In the present paper we will extend our method for profile systems [6] by three steps:

The most important part of the work was the extension to cases of multiple trailing edge separation. This means that simultaneously separation regions are allowed at several parts of the profile system and their interaction is considered. It is only in this way that an exact determination of the maximum lift, and calculation of the lift curve in the post-stall range becomes possible.

In addition, two smaller extensions are made which allows the consideration of short separation bubbles and a consideration of the influence of compressibility for subsonic flow. /11

The extended method is then tested with various examples and new application limits and desirable further extensions are determined.

2. THE CALCULATION METHOD

2.1 Introduction into the previous method [6,6a]

We will first consider the simplest case of a flow around a profile system with separation, that is, incompressible flow with a simple trailing edge separation with a large Reynolds number (Figure 1). It is assumed that only three of the basic elements of the flow field exist, that is, approximately frictionless external flow, the boundary layer at the body contour and a dead water region with almost quiet flow, above and behind one of the profiles. First of all, no additional elements are assumed (for example, separation bubbles and further dead water regions) which could substantially change the flow.

The calculation of such a flow requires the calculation or theoretical modeling of each of the elements and consideration of their interactions.

Our calculation is divided into two main parts which are coupled by iteration:

1) the calculation of a potential flow with enclosed simulated dead water displacement region for a given separation point,
2) boundary layer calculation at the body contour outside of the dead water region for a given pressure distribution.

The coupling is carried out through the pressure distribution and the separation point:

A separation point is found by iteration for which the corresponding potential flow has a pressure distribution where the corresponding boundary layer separates exactly at this point.

Calculation of the potential flow with dead water:

For the calculation of the potential flow, a singularity method with vortex occupation on the body surface is used. In addition, /12
on the profile with separation a source occupation is applied through which an outflow region is generated which is similar to a dead water region in its characteristics regarding the displacement effect with respect to the external flow. For this simulated dead water region, it is required that it has constant pressure along its boundaries near the profile.

After specification of the source occupation $v_n(\phi)$, there is first the problem of determining the vortex occupation $v_t(\phi)$ in such a way that the kinematic flow condition at the body contour is satisfied everywhere. For solving this problem, for the case of a single profile of MARTENSEN and SENGBUSCH [9], the following integral equation of the second kind was derived:

(1)
$$\omega_t(\varphi) - \frac{1}{2\pi}\int_0^{2\pi} K(\varphi,\psi)\,\omega_t(\psi)\,d\psi = 2v_\infty(\dot{x}(\varphi)\cos\alpha + \dot{y}(\varphi)\sin\alpha) + \frac{1}{2\pi}\int_0^{2\pi} L(\varphi,\psi)\,\omega_n(\psi)\,d\psi.$$

For the case of a profile system consisting of N profiles, equation (1) can be extended to the following system of coupled linear integral equations

(2)
$$\omega_t(\varphi_k) - \sum_{j=1}^{N}{}' \frac{1}{2\pi}\int_0^{2\pi} K(\varphi_k,\psi_j)\cdot\omega_t(\psi_j)d\psi_j =$$
$$= 2v_\infty(\dot{x}(\varphi_k)\cos\alpha + \dot{y}(\varphi_k)\sin\alpha) + \frac{1}{2\pi}\int_0^{2\pi} L(\varphi_k,\psi_i)\omega_n(\psi_i)d\psi_i,$$

for $k = 1,2,\ldots,N$.

Here we have:

i number of the profile with separation, along which there is the transformed source occupation ω_n,

j,k running profile numbers

(2a)	$\omega_t(\varphi_k) = v_t(\varphi_k)\cdot\dot{s}(\varphi_k)$	transformed vortex intensity at the point ϕ_k of the profile k
(2b)	$\omega_n(\psi_i) = v_n(\psi_i)\cdot\dot{s}(\psi_i)$	transformed source intensity at the point ψ_i of the profile i
(2c)	$\dot{s}(\varphi) = ds/d\varphi = \sqrt{(dx/d\varphi)^2 + (dy/d\varphi)^2}$	derivative of the running length s along the profile contour with respect to the parameter ϕ

It is assumed that each profile is available in a parameter representation $x(\varphi)$, $y(\varphi)$ so that starting with $\varphi = 0$ at the trailing edge, the profile is passed through exactly once in the counter-clockwise direction for $\varphi = 0$ to 2π.

In equation (2), in addition $K(\varphi,\psi)$ and $L(\varphi,\psi)$ are the influence functions. They are the tangential speed which is produced by unit vortex or unit source which lie at a point defined by ψ, at a contour point defined by ϕ. It is calculated according to the following formulas:

(2d) $$K(\varphi_k,\psi_j) = 2\,\frac{\dot{y}(\varphi_k)\cdot[x(\varphi_k)-x(\psi_j)] - \dot{x}(\varphi_k)[y(\varphi_k)-y(\psi_j)]}{[x(\varphi_k)-x(\psi_j)]^2 + [y(\varphi_k)-y(\psi_j)]^2}$$

(2e) $$L(\varphi_k,\psi_i) = 2\,\frac{\dot{x}(\varphi_k)\cdot[x(\varphi_k)-x(\psi_i)] + \dot{y}(\varphi_k)\cdot[y(\varphi_k)-y(\psi_i)]}{[x(\varphi_k)-x(\psi_i)]^2 + [y(\varphi_k)-y(\psi_i)]^2}$$

The system of integral equation (2) can be transformed by discretization into a set of N linear equation systems which can be solved numerically. One condition for a unique solution is that not only all of the geometric data but also the incident data v_∞ and α as well as the source occupation ω_n on the right side of equation (2) are known. In addition, one additional condition is required for specifying the circulation for each profile.

By the simultaneous solution of the equation system for different right sides and different additional conditions, the so-called basic solutions given in Figure 2 are calculated and with a weighted superposition we finally are able to generate flows of the kind shown in Figure 1. /14

The basic solutions (a_1) and (a_2)(parallel basic flows) are obtained for $v_\infty = 1$, $\alpha = 0°$ and $90°$, $\omega_n = 0$ respectively and the additional conditions $\omega_t(\varphi_k = 0) = 0$ for all k. ($\varphi_k = 0$ means the trailing edge of profile k). Basic solution (b) (pure circulation flow around profile i) is obtained from $v_\infty = 0$, $\omega_n = 0$ and the additional conditions

$$\Gamma_i = \int_0^{2\pi} \omega_t(\varphi_i)\,d\varphi_i \neq 0 \qquad \text{and} \qquad \omega_t(\varphi_k = 0) = 0 \qquad \text{for all } k \neq i.$$

One basic solution (d) (pure outflow) is obtained from $v_\infty = 0$, a source occupation different from 0 * on profile i $\omega_n(\varphi_i) \neq 0$ between A and U and the additional conditions

$$\Gamma_i = \int_0^{2\pi} \omega_t(\varphi_i)\,d\varphi_i = 0 \quad \text{and} \quad \omega_t(\varphi_k = 0) = 0 \quad \text{for all } k \neq i.$$

*) See [10] in section 2.2.1 for the selection of the source occupation.

The basic solutions of the last kind are made available for different positions of $A = A_m$, $m = 1.2,\ldots$ so that it is possible to produce displacement regions of various length by superposition with other basic solutions. The basic solution (d) corresponding to A_m will be called (d_m).

After obtaining the basic solutions it is then necessary to produce a resulting flow by superposition with suitable weighted factors a_1, a_2, b and d_m which have a given incident flow V_∞, α and a displacement region along whose boundary the pressure is constant.

The incident flow is only determined by the basic solutions (a_1) and (a_2) which are the only ones not equal to zero. For $V_\infty = 1$ (reference speed for all speed magnitudes) we find the following for the superposition factors a_1 and a_2:

$$(3) \qquad a_1 = \cos\alpha \qquad \text{and} \qquad a_2 = \sin\alpha.$$

The remaining superposition factors b and d_m of the circulation flow and outflow essentially determine the direction and thickness of the displacement region. They are determined by iteration in such a manner that the resulting flow has equal pressure at three characteristic points, that is, at the two separation points A_m and /15
U and a point O on the upper boundary of the displacement region above the profile trailing edge (see Figure 1). In this way we have satisfied the condition for constant pressure along the boundaries of the displacement region near the profile approximately. Therefore, one has to solve the two equations

$$(4) \qquad c_{pA}(b,d_m) = c_{pU}(b,d_m) = c_{pO}(b,d_m)$$

We will discuss this problem further in section 2.2.2.

Calculation of the boundary layer

After we have obtained a potential flow with a simulated dead water region with a specified attachment point A_m, we must examine whether this flow is physically realistic. It is only when the flow has a boundary layer which separates exactly at A_m that it can really exist. Otherwise, the calculation for different A_m has to be repeated until the correct solution is found. During this iteration process we require boundary layer calculations which will provide reliable solutions which are not too complex. We use the integral method of Rotta in [11] which was programmed.

Our boundary layer calculation always starts laminarly at the front stagnation point and can be continued in a turbulent manner as desired starting at a specified transition point or according to the empirical transition criterion of Michael [10] or it can start from a calculated laminar separation point and this is continued up to turbulent separation. In addition to determining the separation point, the boundary layer calculation is also used to determine the friction drag and the boundary layer displacement thickness δ_1. The boundary layer displacement in our calculation is considered by adding an additional basic solution (d_o) with the source condition

(5a) (5a) $v_n = d(\delta_1 \cdot v_t)/ds, \qquad \omega_n(\varphi_k) = d(\delta_1 \cdot v_t)/d\varphi_k$

and the additional condition /16

(5b) $\omega_t(\varphi_k = 0) = 0$

*

*) Recently, we have preferred the additional condition $\omega_t(\Delta\psi) = -\omega_t(2\pi - \Delta\psi)$ with $\Delta\psi = 2\pi/30$, that is, the condition of equal velocity at two points which lie near the trailing edge at the same distances along the top side of the bottom side.

In later sections we will discuss some new features in further details of the boundary layer calculation.

The overall procedure for the previous method

The overall procedure includes a preliminary phase consisting of two iterations inside of one another and a final calculation: The preliminary calculation contains:

The preparation of all geometric quantities, calculation of basic solutions a_1 and a_2,
calculation of the attached frictionless flow (superposition of basic solutions (a_1) and (a_2) and the corresponding boundary layer and finally the calculation of the basic solutions (b), (d_o), (d_1), (d_2)...

The internal iteration includes:

The calculation of a flow with simulated dead water region for an attachment point A_m at the profile number i. This is done by superposition of basic solutions (a_1), (a_2), (b), (d_0) and (d_m). The determination of suitable superposition factors b and d_m is done by iteration. The purpose of this iteration is to achieve equal pressure at points A_m, U and O.

The external iteration is used to find a flow with simulated dead water region where the attachment point A_m coincides with the separation point A of the boundary layer. In addition to the inner iteration it includes a boundary layer calculation for the top side of profile i for determining the separation point A. Starting with an attachment point near the trailing edge, this is done in small steps and pushed forward until the boundary layer calculation for the first time results in no separation ahead of A_m.

The final calculation contains the following:

Determination of the force and moment coefficients of the profile system by integration of the pressure and shear stress distribution, also boundary layer calculations for the top side and the bottom side of all of the profiles participating in the system. We then find whether as assumed separation actually occurs for a single profile (number i) for the given configuration, incident flow angle and Reynolds number. Otherwise, the calculated flow cannot be looked upon as realistic. /17

2.2 Determination of multiple trailing edge separation

For maximum lift and especially in the post stall range, profile systems often have several separations in regions at various parts of the system. For example, a profile with a highly deflected gap flap will only exceed its maximum lift at an angle of attack for which there is a substantial separation over the main wing for flap separation. In order to allow one to calculate the maximum lift and the post stall behavior for profile systems, it is necessary to expand our method to the case of multiple separation.

In order to be able to not only simulate a profile but in the extreme case to simulate all profiles of the system and their separation regions, suitable source conditions along all profiles are required. This leads to the following expanded integral equation system

$$\omega_t(\varphi_k) - \frac{1}{2\pi}\sum_{j=1}^{N}\int_0^{2\pi} K(\varphi_k,\psi_j)\,\omega_t(\psi_j)\,d\psi_j = R(\varphi_k) \tag{6}$$

for $k = 1,2,\ldots N$

where

$$R(\varphi_k) = 2v_\infty(\dot{x}(\varphi_k)\cos\alpha + \dot{y}(\varphi_k)\sin\alpha) + \tag{6a}$$

$$+ \frac{1}{2\pi}\sum_{j=1}^{N}\int_0^{2\pi} L(\varphi_k,\psi_j)\,\omega_n(\psi_j)\,d\psi_j .$$

As will be discussed in the following sections, this system of coupled linear integral equations allows one to calculate an additional supply of basic solutions which then can be superimposed during an additional iteration method in such a manner that the resulting flow contains several simulated dead water regions. /18

2.2.1 The required basic solutions and their calculation

In addition to the basic solution (a_1) and (a_2) discussed in section 2.1, for each profile i (i = 1.2,...N) we require one circulation flow (b_i) and a set of outflows ($d_{i,1}$), ($d_{i,2}$),...with various attachment points $A_{i,1}$, $A_{i,2}$,...of the source occupation.

We will now exactly define these basic solutions and give the corresponding right sides $R(\varphi_k)$ for equation (6) as well as the additional conditions:

Basic solution (b_i): Source free, circulation flow which vanishes at infinity with specified circulation $\Gamma_i = 2\pi\, l\, V_\infty$ around profile i, which satisfies the Kutta outflow condition at the trailing edge at all other profiles. This means:

$\omega_n(\psi_j) = 0$ for all j

$v_\infty = 0$

$$\int_0^{2\pi} \omega_t(\psi_i)d\psi_i = 2\pi l V_\infty$$

$\omega_t\ (\phi_k = 0) = 0$ for all $k \neq i$.

The first and second conditions substituted in equation (6a) give

$R(\phi_k) = 0$.

The third and fourth conditions are additional conditions for unique calculation of these basic solutions. For each profile, a basic solution of this kind is calculated.

Basic solution ($d_{i,m}$): Outflow which vanishes at infinity which is caused by a specified source condition between contour points $A_{i,m}$ and U_i has no circulation around profile i and satisfies the Kutta outflow condition at all other profiles. This means: /19

$v_\infty = 0$

$\omega_n(\psi_i) \neq 0$ between $A_{i,m}$ and U_i, $\omega_n(\psi_j) = 0$ for $j \neq i$

$$\int_0^{2\pi} \omega_t(\psi_i) d\psi_i = 0$$

$\omega_t(\varphi_k = 0) = 0$ for all $k \neq i$.

The first and second conditions in equation (6a) give

$$R(\varphi_k) = \frac{1}{2\pi} \int_0^{2\pi} L(\varphi_k, \psi_i)\, \omega_n(\psi_i) d\psi_i \,.$$

The source occupation $\omega_n(\psi_i)$ which occurs here is calculated according to equation (2b) and the normal velocity distribution v_n according to Figure 3 is selected (see also [10]).

The third and fourth conditions are again the additional conditions for unique calculation of this basic solution. For each profile, several basic solutions of this kind are calculated (for several attachment points of $A_{i,m}$) on the profile top side.

Numerical solution of the integral equation system

The integral equation system (6) after discretization* gives a linear equation system for each value of k. If M_k is the number of support points $P_{k,\mu}$, $\mu = 1,2,\ldots,M_k$ on the profile k, then the k-th equation system contains M_k equations. All of the N equation systems then give

$$M = \sum_{k=1}^{N} M_k \quad \text{equations}$$

*) Approximation of the integral by sums according to the rectangle rule.

The number of unknown values of vortex intensity $(\omega_t)_{j,\nu}$ at all support points $P_{j,\nu}$, $\nu = 1,2,\ldots, M_j$, $j = 1,2,\ldots,N$ is

$$M = \sum_{j=1}^{N} M_j .$$

Nevertheless, it is not immediately possible to obtain any general unique solution of the overall system because each individual equation system is simply linearly dependent. It is only after one additional condition is added to each of the equation systems that one obtains a unique overall solution. (The summing up of the additional equations for all of the equations of the system has proven itself).

In order to obtain good numerical results with the minimum effort, in earlier work a number of special measures for establishing equation systems were developed, for example, a method for obtaining favorable support point distribution [12], special formulas for better treatment of relatively thin profiles and profiles with corner trailing edges [13] and many other things. In [10], there is a discussion of this. We will not discuss these details again even though they are important for practical success of the method.

By solving the overall system of linear equations for those right sides and those additional conditions which correspond to a special basic solution (g), one finally obtains all of the values of the transformed vortex occupation $(\omega_t)^{(g)}_{j\nu}$ and, therefore, using equation (2a) the tangential speeds $(v_t)^{(g)}_{j\nu}$ at all of the support points $P_{j\nu}$, $\nu = 1,2,\ldots M_j$ of all profiles j = 1.2,...,N for this special solution (g).

In the practical calculation of the tangential speed for our different basic solutions, it is economical to simultaneously solve the linear equation system for all basic solutions in which the equation systems only differ by their right sides (including the additional conditions). This applies for the basic solutions (a_1)

and (a_2) as well as for each group (b_i), $(d_{i,1})$, $(d_{i,2})$,... for a fixed i.

2.2.2 Superposition of basic solutions /21

After we have made available vortex and velocity distribution for all of our basic flows, it is now necessary by means of a suitable weighted supersposition to obtain a resulting flow with simulated separation regions at several profiles, and an equal pressure condition has to be satisfied for each of the separation regions.

The result of a superposition

$$(7) \qquad (v_t)_{j\nu} = a_1 \cdot (v_t)_{j\nu}^{(a_1)} + a_2 \cdot (v_t)_{j\nu}^{(a_2)} + \\ + (v_t)_{j\nu}^{(d_0)} + \sum_{i=1}^{N} [\, b_i \cdot (v_t)_{j\nu}^{(b_i)} + d_{i,m_i} \cdot (v_t)_{j\nu}^{(d_{i,m_i})} \,]$$

depends on the values of the basic solutions and on the selected superposition factors $a_1, a_2, b_{1,m_1}, b_2, d_{2,m_2}$.

For $V_\infty = 1$ and a given outflow angle α, a_1 and a_2 are to be looked upon again as given according to equation (3).

For given attachment points of the separation regions A_{i,m_i}, $i = 1.2,...,N$ the 2 N additional superposition factor B_i and d_{i,m_i}, $i = 1.2,....N$ are to be found in such a manner that the pressure coefficients

$$(8) \qquad c_p = 1-(v/V_\infty)^2 = f(b_1, d_{1,m_1}, b_2, d_{2,m_2}, \ldots, b_N, d_{N,m_N})$$

are the same at the comparison points A_{i,m_i}, U_i and 0_i of each separation region. In other words, the common zero of the two N functions

$$(9) \qquad \begin{aligned} c_{pA_{i,m_i}} - c_{pU_i} &= g_i(b_1, d_{1,m_1}, \ldots, b_N, d_{N,m_N}) \\ c_{pU_i} - c_{pO_i} &= h_i(b_1, d_{1,m_1}, \ldots, b_N, d_{N,m_N}) \end{aligned} \qquad i = 1,2,\ldots,N$$

is to be determined.

The values of the function g_i can be easily calculated for a given set of superposition factors using equations (7) and (8). The calculation of the function values of h_i is more complicated. First of all, the field points 0_i along the upper boundaries of the separation regions have to be determined and the velocities there v_{0_i} have to be calculated. /22

The velocity components v_x and v_y at an arbitrary field point P(x,y) are calculated from the following formulas:

(10a) $$v_x(x,y) = V_\infty \cdot \cos\alpha + \sum_{j=1}^{N} \frac{1}{M_j} \sum_{\nu=1}^{M_j} \frac{(x-x_{j\nu})(\omega_n)_{j\nu} - (y-y_{j\nu}) \cdot (\omega_t)_{j\nu}}{(x-x_{j\nu})^2 + (y-y_{j\nu})^2}$$

(10b) $$v_y(x,y) = V_\infty \cdot \sin\alpha + \sum_{j=1}^{N} \frac{1}{M_j} \sum_{=1}^{M_j} \frac{(y-y_{j\nu})(\omega_n)_{j\nu} + (x-x_{j\nu})(\omega_t)_{j\nu}}{(x-x_{j\nu})^2 + (y-y_{j\nu})^2} .$$

A field point 0_i can now be found by starting at a point near to A_{i,m_i} and following the speed direction (streamline), until one has reached the desired position above the profile trailing edge. Then one obtains v_{0_i} from $v^2 = v_x^2 + v_y^2$.

Now that we are in the position of numerically calculating the values of the functions g_i and h_i according to equation (9) for a given set of superposition factors $b_1,\ldots,d_{N,m_N}$, we will now consider the determination of the zeros.

We have to find a set of superposition factors so that

(11) $$\begin{aligned} g_i(b_1, d_{1,m_1}, \ldots, b_N, d_{N,m_N}) &= 0 \\ h_i(b_1, d_{1,m_1}, \ldots, b_N, d_{N,m_N}) &= 0 \end{aligned} \quad \text{for} \quad i = 1,2,\ldots,N$$

The solution of this problem is done using an iteration and recourse to physical interpretation. First of all, we assume that reasonable zero solutions are available for the superposition factors $b_1^{(o)}, d_{1,1}^{(o)}, \ldots, b_N^{(o)}, d_{N,1}^{(o)}$, and we will discuss this at the end of this section.

We start the entire iteration calculation with small separation regions at all profiles, that is, with attachment points $A_{i,1}$ which are only a few per cent of the profile chords away from the trailing edges*. In this case, one can expect that the mutual influencing of the separation regions is small and, therefore, the correct value pair b_i, $d_{i,1}$ will barely depend on the other ones. /23

Each value pair b_i, $d_{i,1}$ is then calculated using a two-dimensional Newton method (see [6a], and for all of the other superposition factors, the previously highest approximations are used and fixed:

$$b_i^{(n)}, d_{i,1}^{(n)} \quad \text{and the highest approximations of } b_j, d_{j,1} \text{ for } j \neq i$$
$$\longrightarrow b_i^{(n+1)}, d_{i,1}^{(n+1)} \qquad , \quad n = 0,1,2,\ldots$$

As soon as this iteration is finished, the next profile is calculated: i = 1.2,...,N. The result of this iteration are improved approximations $b_1', d_{1,1}', \ldots, b_N', d_{N,1}'$ of all of the superposition factors. But in the calculation of, for example, $b_1', d_{1,1}'$, only the zero approximation of the other superposition factors were available. "A second run through this iteration may be useful (after substitution of the zero approximations with new values) (especially if the separation regions are large and the zero approximations were not very good).

Using the selected superposition factors, the resulting overall flow is known. If it is necessary to make calculations for additional attachment points A_{i,m_i} (that is, larger separation regions) (see section 2.2.3), then this can be done in the same way as for

*) We selected the first attachment point $A_{i,1}$ as well as the attachment point U_i on the lower side at about 98.5% of the profile chord.

the attachment points $A_{i,1}$. One requirement is that we will always have a good zero approximation for superposition factors

$$b_1^{(o)},\ d_{1,m_1}^{(o)}, \ldots, b_N^{(o)},\ d_{N,m_N}^{(o)}$$

This is done by allowing the attachment points A_{i,m_i} with $M_i = 1,2,3,$ ...to only advance a small step and for each new set of attachment points we will use the results of the previous calculation as the zero approximation for the superposition factors:
New $b_i^{(o)}$ = previous b_i' and
new $d_{i,m_i}^{(o)} = d'_{i,m_i-1}$ and previous d'_{i,m_i}, depending on whether for profile number i the attachment point was displaced forwards or not.

At the end of this section we will now discuss how reasonable zero approximations of the superposition factors can be obtained for the first attachment points lying near the trailing edges. /24

If the displacement region near the trailing edge H_i has the height h which is simulated by the outflow region (see Figure 4) and the average speed of the outflow is approximately V_∞, then approximately the following relationship has to hold:

(12a) $V_\infty \cdot h = d_{i,1} \cdot E_{i,1}$ where

(12b) $E_{i,1} = \int_{\varphi_{U_i}}^{\varphi_{A_{i,1}}} \omega_n(\psi_i)\,d\psi_i$ is the yield of the source occupation

With our selected source occupation, the yield is $E_{i,1} \approx 0{,}7 \cdot V_\infty \cdot t$. "For small displacement regions, then from equation (12a) we find $d_{i,1} \approx (h/t)/0.7$. if we use the estimate h/t = 1.2,...,N, we obtain

(13) $$d_{i,1}^{(o)} \approx 0{,}6\ ;\ i = 1,2,\ldots,N.$$

We will select the superposition factor $b_i^{(o)}$ in such a way that the resulting overall flow provides for smooth departing flow at the trailing edge H_i of each profile i:

$$\omega_{tH_i} = a_1\omega_{tH_i}^{(a_1)} + a_2\omega_{tH_i}^{(a_2)} + b_i\omega_{tH_i}^{(b_i)} + d_{i,1}\omega_{tH_i}^{(d_{i,1})} +$$

$$+ \sum_{\substack{j=1 \\ j\neq i}}^{N} [b_j\omega_{tH_i}^{(b_j)} + d_{j,1}\omega_{tH_i}^{(d_{j,1})}] = 0. \tag{14}$$

Based on the additional conditions selected for the basic solutions, all of the $\omega_{tH_i}^{(g)}$ are zero, with the exception of $\omega_{tH_i}^{(b_i)}$ and $\omega_{tH_i}^{(d_{i,1})}$. Therefore, equation (14) gives

$$b_i^{(0)}\ \omega_{tH_i}^{(b_i)} + d_{i,1}^{(0)}\ \omega_{tH_i}^{(d_{i,1})} = 0$$

/25

Using equation (13) we find

$$b_i^{(0)} = -0,6 \cdot \omega_{tH_i}^{(d_{i,1})} / \omega_{tH_i}^{(b_i)}, \qquad i = 1,2,\ldots,N.$$

We now have the required approximation values for the first iteration.

2.2.3 Finding separation point

After calculating the resulting flow with the separation regions behind the attachment points $A_{1,m_1}, A_{2,m_2}, \ldots, A_{N,m_N}$ boundary layer calculations are carried out for the top sides of all profiles. For each profile i these determine whether the boundary layer would separate for this flow ahead of A_{i,m_i}. If this is the case, then for the corresponding profile the point 6 is considered as new attachment points for the next calculation which should lie a small distance ahead of it; otherwise, the previous attachment point is retained. Our attachment points are placed along the upper side support points along the profile contours in such a manner that when m_i is increased by 1, the attachment point moves to the next forward support point by a small amount.

The overall calculation is repeated for a new set of attachment points. This is repeated until a set is found for which the resulting flow for the first time no longer has any separation ahead of any of the attachment points. This flow is the result of our calculation. Since for the attachment points just behind them, separation would have resulted ahead of these points now that it no longer occurs, one would expect that the last used attachment points will agree with the desired and physically correct separation point. One has to determine, however, whether one can justify always moving forward when finding the correct set of attachment points of the separation region (or whether one should stand still). We, therefore, have assumed that an increased separation at one of the profiles will also result in an intensified separation at the other profiles (or at least it will stay the same), but will never result in a reduced separation. Let us consider the most important case in practice of a slat-main wing -- slotted flap combination with the following possibilities: /26

(a) intensified separation at the flap:

Because of the reduced flap effect (reduced speed at the rear part of the main wing topside) intensified separation can be expected over the main wing.

(b) intensified separation at the slat:

Because of the reduced slat effect (reduced unloading of the main wing in the front part, higher suction peak) intensified separation can be expected over the main wing.

(c) intensified separation over the main wing:

The reduced circulation over the main wing again gives a flow which has a reduced inclination but a slower flow in the region of the slat and a flow with higher inclination in the region of the (extended) flap. For the flap it is not certain which effect dominates but for the flap, intensified separation can be expected.

From (b) and (c), we finally find the indirectly intensifying influence of a slat separation on the flap separation.

This means that with some care the assumption made above for a tendency of alternating intensification of the separation regions can be accepted.

The other question has to be posed: Is the final solution found with the method described the only possible one or only that solution with the smallest possible separation regions?

The question of whether there are physically correct solutions with larger separation regions will be discussed in section 3.4 for several calculation examples. When looking for the separation points, we will use the methods discussed above as well as the reverse method by starting with very large separation regions. The attachment points will be displaced backwards in small steps until for the first time separation occurs ahead of all attachment points. In this way we will determine the solution with the largest possible separation region. We should report here that for all of the investigated cases, the solutions with the smallest possible and the largest possible separation regions approximately agree, that is, the solution was unique.

2.2.4 Closed dead water model for improving the dead water pressure calculation and drag calculation /27

In [10] for a single profile it was found that a certain improvement to the calculated results can be achieved, especially for the dead water pressure and for the drag, by transferring from the open dead water model to a dead water model with finite length. This is achieved by applying an additional sink at a suitable position behind the profile.

For our profile systems with multiple separations, this procedure improvement is only partially adapted. In order to avoid complication, a refined dead water model is only used for the profile of the system which is the farthest downstream.

2.3 Consideration of separation bubbles

In addition to the previously treated trailing edge separation which expands from the trailing edge with increasing inclination and has a displacement region which extends above the trailing edge, the separation can also occur in the form of so-called separation bubbles in which the separation region is limited by a reattachment of a flow along the profile contour. One distinguishes short and long separation bubbles.

Short separation bubbles have a length of a maximum of only a few per cent of the profile chord length, are rather thin and have no important displacement effect. They can influence the flow in two ways: First of all, by changing the boundary layer and, therefore, the trailing edge separation. Secondly, by a sudden bursting which can generate a large separation region and, therefore, a substantial lift loss. Short bubbles are caused by laminar separation and turbulent reattachment of the flow. According to experience, they occur for medium Reynolds numbers at profiles with moderate thickness and slight curvature along the profile topside near the nose. /28

In [14] it is shown for a single profile how the short bubble can affect the trailing edge separation approximately. This is done by using empirical criteria for the occurrence and bursting of short bubbles, as well as empirical formulas for the bubble length and the initial values of turbulent boundary layer behind the bubbles (detail see [14]). These criterion formulas all contain parameters at the laminar separation point LA $[(v_t)_{LA}, (\delta_2)_{LA}, (\Delta v_t/\Delta s)_{LA}]$, which are available after the conclusion of the laminar boundary layer calculation.

The extension of the method could occur alone within the framework of the boundary layer calculation:

During the calculation of the laminar boundary layer, it is examined whether transition has occurred. If not, then at the laminar separation point LA, it is examined whether a short bubble can exist. If this is the case, then its length l_B is calculated and the turbulent boundary layer calculation is started only at a distance l_B behind LA. The momentum and energy loss thickness of LA are used as initial values. Otherwise, the turbulent boundary layer calculation is started at the transition point or at LA. If bursting of the bubble can be expected, then LA is assumed to be a turbulent separation point.

The expanded boundary layer program was used in our profile system calculations. If a short bubble exists, one usually obtains a somewhat reduced trailing edge separation and, therefore, a somewhat larger lift.

Long bubbles can extend over a large part of the profile chord, can be very thick and can have a substantial direct displacement effect on the external flow. If such bubbles are on the profile topside, which especially occurs for thin profiles or small Reynolds numbers, then there is a lift decrease and drag increase. Reliable calculation methods for such bubbles are not yet available. For profile systems especially at higher Reynolds numbers, such topside large bubbles probably occur rarely. More often large bubbles occur along the profile bottomside and when they separate, they are triggered at the specified points with large curvature (for example, at the slat bottomside and at the beginning of the flap cavity). Such bubbles on the bottomside can substantially change the pressure distribution, but usually are not very important for the overall flow and the lift. They can be considered with estimated contour modifications to sufficient accuracy. We will discuss this in section 3.2. /29

2.4 Consideration of compressibility

High lift systems are being used for low speeds (the Lande-Mach numbers of large commercial aircraft are $Ma_\infty \approx 0{,}20$)). Because of local over-speeds, compressibility influences can be felt already for incident Mach numbers starting with $Ma_\infty \approx 0{,}1$. For a pure subsonic flow, because of increased pressure gradients, the trailing edge separation is somewhat increased and, therefore, there is a reduction in the lift. Local supersonic regions and compression shocks can occur already starting at $Ma_\infty \approx 0{,}20$

We will now consider a relatively simple compressibility correction and will restrict ourselves to pure subsonic flow. This was developed in [15] and was successfully used for single profiles.

After obtaining the final solution for incompressible flow with separation, the pressure coefficient $c_{p\ ink}$ is recalculated according to [15] using the approximate formula

$$c_{p\ ink.} = 1 - \left[1 + \frac{2}{\kappa - 1} \frac{1 - \left(1 + \frac{\kappa}{2} Ma_\infty^2 c_p\right)^{(\kappa-1)/\kappa}}{Ma_\infty^2} \right] \cdot \left(1 + \frac{\kappa}{2} Ma_\infty^2 c_p\right)^{0.72/\kappa} \tag{15}$$

to find the pressure coefficients c_p in the compressible flow. (The calculation of c_p from this equation is done by iteration by solving the equation $c_{p\ ink.} - f(\kappa, M_\infty, c_p) = 0$ using the Newton method). Using the pressure coefficients corrected in this way, the boundary layer calculation is again carried out with consideration of the compressibility. The search for the physically correct solution is continued if separation now occurs ahead of at least one dead water attachment point.

In order to avoid cases where the given incident Mach number is over-critical during each compressibility correction it is examined whether the pressure coefficient $c_{p\ ink}$ is less than the value /30
$c^*_{p\ ink}$

using equation (15) corresponding to the critical pressure coefficient

$$c_p^* = \frac{2}{\kappa Ma_\infty^2} \left[1 - \left(\frac{2}{\kappa+1} + \frac{\kappa-1}{\kappa+1} Ma_\infty^2 \right)^{\frac{\kappa}{\kappa-1}} \right] \tag{16}$$

anywhere. In this case, the Mach number is reduced until everywhere we have $c_{p\ ink.} \geq c^*_{p\ ink.}$. In the case of a given over-critical Mach number, the critical Mach number is determined and the calculation is carried out for it.

3. METHOD TESTING AND IMPROVEMENT TESTS

In order to test our calculation method, its application limits and possible improvements, numerous examples were calculated and the theoretical results were compared with measured results as far as possible.

3.1 First results for a profile with Fowler flap

The first flow calculations were done for the profile GA(W)-1 with a 30% deep Fowler flap, for which experimental investigations were described in detail in [16,17]. This included force measurements, pressure distribution measurements and flow visualizations for various flap positions and angles of attack, but for moderate Reynolds numbers (between Re = $2 \cdot 10^6$ and Re = $3 \cdot 10^6$). The Mach number was $Ma_\infty \approx 0{,}15$. In order to fix the laminar-turbulent transition, turbulent strips were used for all measurements which were attached at 5% profile chord along the topside and the bottomside of the main wing.

Figure 5 shows the lift curves according to theory and experiments in the case of deployed flaps with 30% flap deflection and for comparison also for the case of the retracted flap (single profile). The Reynolds number was $2.2 \cdot 10^6$. For the calculations, it was first assumed that there were no separation bubbles on the topside and that the transition occurs at the laminar separation point but at the latest at the location of the turbulent strips, and also that the flow was incompressible ($Ma_\infty = 0$). For the case of the deflected flap, for small to moderate angles of attack there is a good agreement between the theoretical curve and the experimental value (symbols). In particular, it is found that the substantial increase in the lift compared with the single profile as well as the lift loss (caused by friction and partial separation) as compared with ideal flow is well represented by our theory. The maximum lift coefficient is substantially increased by the deployed flap as follows: /31

according to measurements from about 1.55 to about 3.6 and according to theory from about 1.50 to about 3.8.

This result is somewhat satisfactory as well. On the other hand, in the post stall range, the results are not satisfactory for the present profile system. We will discuss this later.

By consideration of the compressibility (dashed curves), the results were somewhat improved but not drastically.

The following observations are unsatisfactory.

a) For the single profile at moderate angles of attack, the measured lift coefficients are clearly higher than the calculated ones. This could be caused by the fact that here short separation bubbles occur in practice in spite of the turbulent strips which already occurred ahead of the turbulent strips. A second calculation where short separation bubbles are allowed resulted in the thin curve shown. According to this, such bubbles seem to also exist for moderate angles of attack but not in the post-stall range. Our empirical criterion for the existence of bubbles also gave short bubbles in the post-stall range but is unreliable here.

b) For the flap profile in the post-stall range, the calculated lift coefficients are much higher than the measured ones. In the

present example physical phenomena must come into play, which are not completely covered in the theoretical model yet. In order to obtain a better insight into the physical reality, in Figure 6 we show the pressure distribution of the flap profile for $\alpha = 10.3^\circ$ and 12.8%. At $\alpha = 10.3$, the theory and the measurement have only small /32
separations over the main wing. At the flap our calculation results in moderate trailing edge separation, whereas the measured pressure distribution indicates a separation bubble near the nose. Overall, the pressure distributions agree for the most part.

At $\alpha = 12.8^\circ$ on the other hand, the measurement at the flap shows a remarkable pressure distribution. It deviates from the pressure distribution for the flow without separation (dashed curve) as well as from the pressure distribution calculated for trailing edge separation (solid curve) to a significant degree. Apparently, we have no clear trailing edge separation here but a very strong influence of friction. Perhaps this is a long bubble with adjacent very thick boundary layer. Over the main wing the measurement shows clear trailing edge separation with substantial dimensions, whereas the calculated flow is approximately attached. The unrealistic modeling of the flap flow here apparently leads to a false result with respect to the position of the separation point over the main wing.

Clear agreement in the pressure distribution over the main wing, on the other hand, occurs when the position of the separation point is correctly specified there (solid curve in Figure 7)*. For the entire flow in this case, the lift coefficient of $c_a = 2,9$, results which is not very different from the measured one. At the flap the calculation gives 50% trailing edge separation with a

*) For the calculation the computer program was extended so that the iteration determination of the separation points could be selected for those profiles, for which no fixed specified separation points were available.

pressure distribution which is clearly different from the measured one.

In order to examine to what extent the modeling close to reality of the flap flow might lead to a better overall solution, we attempted to achieve a pressure distribution over the flap with a suitable contour modification which is close to the measured one. The result is the dashed curve in Figure 7. Automatically, we found a stronger separation and a better pressure distribution over the main wing and a lift coefficient of $c_a = 2.6$ which almost agrees with the measured one. This means that we would be in the position of /33
calculating the overall flow even for substantial separation over the main wing (that is, in the post-stall range), if we were only able to analyze the flow over the flap better. For this purpose, we would have to have more information about how the measured pressure distribution comes about over the flap and we would have to know the responsible physical phenomena. The following possibilities should be considered:

a) long bubble over the flap topside
b) insufficient modeling of the main wing wake and possible contact of this wake with the flap boundary layer (wake boundary layer confluence)
c) influence of separated flow at the flap cavity on the flow around the flap.

Better information about the true condition can only be obtained with very careful experimental work on the flow field in the vicinity of the flap. In the present case, we could not progress using theory alone. It is possible that the complications are caused for the most part by the relatively low Reynolds numbers of the measurement and the special geometry of our example. For large Reynolds numbers over 10^7 which are important for large aircraft, topside separation bubbles probably would no longer occur and the friction effects would be in general smaller. This fact and somewhat larger gap dimensions between the main wing and the flap make a wake-boundary layer confluence less probable. Therefore, we should expect that our method in its present form (that is, without consideration of phenomena mentioned in a) and b)) will give better results for large Re and more favorable configurations.

3.2 The problem of flap cavity flow

Along the bottom side of the main wing at the beginning of the flap cavity there is a corner or at least a strong curvature. In both cases one would expect separation of the flow. For the reflected flap, the flow which is directed upwards ahead of the flap is probably reattached again. In the flap cavity, therefore, we expect a separation bubble. In order to estimate the displacement /34
effect of such a bubble, we carried out calculations for two extreme assumptions as follows:

a) for infinitestimally small bubbles (the original small contour of the flap cavity was used as the profile contour)

b) for a thick bubble whose contour corresponds to the retracted flap (the original profile GA(W)-1 without flap cavity was used as the main wing in the calculation).

The pressure distributions α = k9,3° for both cases are compared in Figure 8 and the measured ones. It can be seen that the bubble only has a local influence on the pressure distribution. It can also be seen that the simple assumption of a bubble which has the shape of the retracted flap already leads to a rather usable correction of the pressure distribution along the bottomside of the main wing. This assumption was, therefore, retained for all previous calculations*.

Regarding the displacement effect, it seems that a very accurate modeling of the flap cavity bubble does not seem to be necessary.

*) Using a somewhat shorter bubble, which reattaches at about 5% ahead of the trailing edge and which has a maximum convex curvature at x/l=0.75, one obtains a slightly better matching to measured results.

On the other hand, other influences should not be excluded, for example, that the transition zone between the bubble and the external flow extends down to the flap boundary layer and it is influenced (due to increased total pressure and/or the change turbulence of the incoming flow). Also there is the possibility of unsteady separation in the flap cavity, especially for a continuous transition. Extensive experimental work about these questions would be very interesting in order to obtain more knowledge and to improve the theoretical model.

3.3 Testing of various trailing edge conditions for calculating the dead water region

As mentioned in section 2.2, we used the following two conditions for specifying the circulation and the displacement for each profile

(17 a,b) $c_{pA} = c_{pU}$ and $c_{pU} = c_{pO}$

A and U were the topside and bottom side separation points and O was the point on the upper boundary of the displacement region. U was always assumed at 98.5% of the profile chord and O was assumed at a distance $\overline{AH}$ from A on the streamline which starts at A. There is a certain arbitrariness in the selection of points U and O. /35

Using a few examples, we examined whether by changing the conditions mentioned above the result of our calculations would be substantially influenced and whether they could then be improved. We were primarily interested in the correct lift value and also in an improved determination of the dead water pressure which was usually too high in our previous calculations. The test calculations were first performed for the profile GA(W)-1 (with a retracted flap). First of all, we varied the position of the lower comparison point U as follows (see also Figure 9):

1) $U \equiv U_{97}$, that is point U at 97% of the profile chord along the bottom side profile contour,

2) $U \equiv U_{98}$, that is point U at 98.5% of the profile chord along the bottomside contour

3) $U \equiv U_{101}$; point U is 1% behind the profile along the extended profile central line.

Figure 9 shows the results of test calculations for $\alpha = 8°$ (slight separation) and $\alpha = 16°$ (moderate separation). First of all, one can see that compared with the theory of frictionless flow, our theory with friction separation in every case results in a substantial improvement.

The different position of the point U brings about slight changes in the results for small separation regions ($\alpha = 8°$) and somewhat larger differences for large separation regions ($\alpha = 16°$). Regarding the pressure distribution outside of the dead water region and regarding the lift, best agreement with the measurements occurs for $U \equiv U_{98,5}$. The position of the separation point A is well calculated, but the value of the dead water pressure is clearly too high in all cases. $U \equiv U_{101}$ at $\alpha = 16°$ gives the most favorable dead water pressure, but leads to a lift coefficient which is clearly too high. In addition, sometimes there are convergence difficulties with $U \equiv U_{101}$. /36

Additional test calculations of this kind were performed with the profile NACA 4415. They confirm the above. The most important input data and results are given in the following table.

PROFILE NACA 4415 Re = $3 \cdot 10^6$, $Ma_\infty < 0.15$ (calculation for: incompressible flow, transition in the lam. separation point)					
α	Lift coefficient c_a according to:				
	theory without friction	measurement from [18]	theory with friction and separation $U \equiv U_{97}$	$U \equiv U_{98.5}$	$U \equiv U_{101}$
8°	1.52	1.20	1.27	1.26	1.25
14°	2.24	1.40	1.37	1.39	1.45

The table again shows a very slight dependence of the result on the position of the point U at $\alpha = 8°$ and only a moderate dependence at $\alpha = 14°$. The most favorable result is again obtained for $U \equiv U_{98,5}$.

In this way we calculated the complete lift curves for two different Reynolds numbers and these are compared in Figure 10 with measurements.

Even though the lift can be easily calculated (as well as the separation point), there is still the problem of the excessively high dead water pressure. For large dead water regions, this is important for the moment and the drag. For the moment curves shown on Figure 10 bottom, we find good agreement between the theory and the measurement only up to $\alpha \approx 12°$, , and beyond this the calculated moment is too large.

Our attempts to change the conditions (17a,b) in order to obtain better results were continued.

As the next step, we varied the position of the point O by changing the distance $\overline{AO}$. Calculations for the profile NACA 4415 gave the following for $Re = 3 \cdot 10^6$ and $\alpha = 14°$. /37

for	$\overline{AO}$	=	$0,9\ \overline{AH}$	$1,0\ \overline{AH}$	$1,1\ \overline{AH}$	measurement
values	c_a	=	1,390	1,392	1,393	1,410
and	$c_{m\,1/4}$	=	-0,020	-0,021	-0,021	-0,070

It is found that the results are rather insensitive to a moderate variation in the position of O and that the lift agrees very well with measured values for all cases. Therefore, we cannot bring about a substantial improvement in the moment coefficient in this way.

It is found that the results are rather insensitive to a moderate variation in the position of O and that the lift agrees very well with measured values for all cases. Therefore, we cannot bring about a substantial improvement in the moment coefficient in this way.

Finally, the conditions (17a,b) were replaced by

(18a, b) $\qquad c_{pA} = c_{pO} \qquad$ and $\qquad v_{tH} = 0,$

In other words, equal pressure is only assumed for points A and O and the requirement for equal pressure in U is given up and replaced by the requirement for smooth departing flow at the trailing edge. The idea of this is to avoid the coupling of the dead water pressure and the relatively high pressure along the profile bottomside. Calculations with these conditions gave the following for the profile NACA 4415 at $Re = 3 \cdot 10^6$ and $\alpha = 14°$

$$c_a = 1.440$$

$$\text{and} \quad c_{m\,1/4} = -0.031.$$

Here we find an improved moment coefficient which is still not satisfactory at a somewhat higher lift coefficient. Calculations for additional angles of attack showed that the same is true for larger angles of attack, but for smaller angles of attack, the conditions (17a,b) and (18a,b) give practically the same good results.

Since we do not have anything better, we will continue to use the conditions (17a,b), that is $U = U_{98.5}$ and $\overline{AO} = 1.0 \cdot \overline{AH}$.

The investigations in this section showed us that the lift is usually calculated correctly and it changes only slightly when one varies U and O moderately. The problem of the excessively high dead water pressure and moment coefficient for large angles of attack, however, remain. We can probably only find a remedy by /38
using a fine dead water model. The model of DVORAK and MASKEW [18] seems promising where the boundaries of the displacement region are represented by vortex layers.

3.4 Various methods for finding separation points and investigations about the uniqueness of the solution

We will now discuss the question whether the separation points which are obtained for the searching method discussed in section 2.2.3 for profile system are the only possible ones. It is hardly possible to give a general proof of this. However, there is one way to clarify the question of a unique solution for a single individual case. If one accepts the principle of mutual intensification of separation regions, then the previous method (search method 1) for which the search starts with very small separation regions, will lead to the solution with the smallest possible separation regions compatible with one another. Conversely, one will obtain the solution with the largest possible separation regions compatible with one another if one starts the search with very large separation regions and if displacement points are displaced in very small steps backwards until, for the first time, separation is established ahead of all attachment points (search method 2). If calculations are made according to both search methods and if both result in the same solution (approximately), then this solution is unique. Strictly speaking, if a unique solution existed, search method 2 should lead to a somewhat smaller separation region than search method 1 because the attachment points A were displaced in finite steps, forwards in the case of search method 1 until they were just ahead of the separation points. For search method 2, they were displaced backwards until they were all just behind the separation point.

After an appropriate program extension, calculations were made according to both search methods for several examples. Figure 11 shows the results for our GA(W)-1 profile with 30% Fowler flap and for 30% flap deflection and $\alpha = 16°$. We show the positions of the attachment point for each iteration step. As expected for the case of a unique solution, the attachment points for both profiles for search method 2 are somewhat behind those found for search method 1. A solution with larger dead water regions, therefore, does not /39 exist.

In the same way two further cases with multiple separation were investigated, that is
the slat-main wing configuration of Figure 13 for
$Re = 3,3 \cdot 10^6$, $Ma_\infty = 0$, $\alpha = 36°$ (strong separation over the main wing, slight separation over the slat), and
the three part configuration consisting of slat, main wing and flap of Figure 14 for $Re = 1,5 \cdot 10^7$, $Ma_\infty = 0$, $\alpha = 20°$ (strong flap separation, small separations over the slat and the main wing).

In both cases we found uniqueness of the solution.

With the assumption that the solution is always unique, of course only a single search method has to be used. Search method 1 should then be preferred because, compared with search method 2, it usually requires less computation time. Also, search method 2 sometimes has convergence difficulties in the iteration calculation of the superposition factors.

In the calculations with slats it was found that the principle of mutual intensification of separation regions is only partially applicable for the slat. The slat separation does influence the separation over the main wing but conversely, for substantial main wing separation there is a somewhat reduced slat separation*. From this the requirement arises for extending the search method in such a manner that the dead water points can migrate not only forwards during the search process, but if necessary, also backwards. This was brought about by using search method 2 after using search method 1 with the found attachment points. Starting with its result, finally search method 1 is used again. In this way by searching forwards, backwards and forwards, the correction to those separation regions is brought about which would be too large if only search method 1 or 2 were used individually.

*) Explanation: Reduced circulation over main wing results in a smaller effective angle of attack of slat.

For our three part configuration, Figure 12 shows the iteration for the combined search method.

The following table gives the positions of the dead water points along the various wing parts according to the various search methods.

	slat	main wing	flap	
$x_A/ =$	-0.025	0.862	1.037	according to search method 1
	-0.020	0.872	1.037	according to combined search method (1-2-1)
	-0.000	0.880	1.052	according to search method 2

As expected, search method 2 always gives values which are somewhat too large (that is, separation regions are too small). There are differences between the results of search method 1 and the combined search method only for the slat and the main wing and they are not large.

For safety, in the following we will always use the combined search method. There is a possibility of reducing the calculation effort as will now be discussed.

In Figure 12, it becomes apparent that the steps should be substantially increased during phase 1 of the searching process. This probably is acceptable for the combined search method as well because in this way the true separation point is clearly exceeded and because this can again be connected by the backward searching in phase 2. On the other hand, it has to be considered that for large steps, the superposition factors b and d will change drastically from step to step so that for the inner iteration (determination of the superposition factors) the zero approximation values will be not as good and, therefore, one would expect higher computational times and even convergence difficulties. It does not seem possible to give general information about the optimum step size with respect to the overall computation time, but by carefully adjusting the step size during search phase 1, a reduction in the overall computational time can probably be brought about. Therefore, for the present example, we carried out sample calculations with the double and triple step size. Both calculations gave the same results as for simple step size (without convergence difficulties). The overall computational time (using the IBM 370/158 computer) were the following: /41

for the combined search method		
with simple step size	19	minutes CPU time
with double step size	17.5	" "
with triple step size	<u>16.6</u>	" "
for search method 1	18	" "
for search method 2	26	" "

Accordingly, the combined search time with the triple step size is the most favorable. A further increase in the step size does not bring about any substantial calculation advantages but increases the danger of convergence difficulties for the inner iteration. The possible calculation time gained by further improvement of the search method is too limited because most of the total calculation time (about 14 minutes in the present case) is required outside of the search process, especially for the calculation of the basic solutions.

For the further calculation we use the combined search method with the triple step size during search phase 1 (and simple step size during the other phases).

At this point we would again like to point out that in the case $Ma_\infty \neq 0$ the compressibility correction (according to section 2.4) is used in the last two search phases whereas the (rough) search phase 1 is only carried out for incompressible flow in order to save time.

3.5 Calculation results for profile with slat

For the two part configuration consisting of slat and main wing investigated experimentally in [20], Figure 13 shows the lift curve according to theory measurements for $Re = 3.4 \cdot 10^6$ and $Ma_\infty = 0.16$ for the two gap widths s. For comparison, we also show the lift curve for the fast flight profile NACA 64-210 without slat. The measured and calculated maximum lift coefficients agree in all cases very well. Both the substantial lift gain with /42 the slat as well as the slight displacement of the lift maximum with the change in the gap are well predicted. In the post-stall range, on the other hand, the calculated lift coefficients are always somewhat higher than the measured ones.

The lift maximum is exceeded also when a slat exists due to advancing separation over the main wing. The small separation over the slat only starts to expand above $\alpha \approx 35°$. For the calculations, it was, therefore, assumed that no bubbles exist and that the transition occurs at the laminar separation point. For the main wing, we used $M_1 = 120$ target points and for the slat we used $M_2 = 60$ for target points. The calculation time on the IBM 370/158 was 7-11 minutes per angle of attack, depending on angle of attack (and, therefore, separation regions).

3.6 Calculation results for a three-part profile system

For a three-part high lift configuration consisting of slat, main wing and Fowler flap designed at the DFVLR Institute for Design Aerodynamics, pressure distributions and lift curves were calculated. Measurements for these configurations are in preparation but experimental results are not yet available.

Calculations were first done for rather large Reynolds numbers ($Re = 1.5 \cdot 10^7$), as might occur during takeoff and landing of large cruise aircraft. Figure 14 shows the configuration and the calculated pressure distribution for $\alpha = 0°$ and $\alpha = 20°$ (corresponds approximately to $c_{a\ max}$). For $\alpha = 0°$, there was a substantial separation on the topside only over the flap. But the following boundary layer calculation which is also carried out for the bottomside of the profile, shows turbulent separations at the bottomsides of the slat and the main wing. With the assumption that in this way long bubbles are created in the slat bottomside and in the slat cavity, the calculation was again repeated with the corresponding modified profile contours. The resulting pressure distribution is also shown in Figure 14 and shows the displacement effect of such bubbles on the bottomside. Substantial changes in the pressure distribution only occurred near the bubbles. Over the flap there was only a slight enlargement of the suction peak. The separation points and the total lift coefficient practically did not change*. /43

For $\alpha = 20°$ on the topside, there was a strong separation at the flap and in addition, no separations over the main wing and the flap, whereas on the bottomside there was no separation. As Figure 15 (top) shows, as the angle of attack is increased further ($\alpha > 20°$), there is an intensification of flap separation and a rapid increase in the separation over the main wing, and therefore, a reduction in the lift coefficient. The separation over the slat first increases slightly and then decreases slightly again for larger angles of attack. Figure 15 shows the various lift curves in the lower part. Except for $Re = 1.5 \cdot 10^7$, the lift curve was also calculated for Reynolds numbers which can be achieved in the wind tunnel ($Re = 6 \cdot 10^6$). There is a strong influence of the Reynolds number on the maximum lift of these high lift configurations. Accordingly, for the full scale version, one would expect about 13% higher lift coefficient than for model measurements in the wind tunnel, provided that in both cases there were no physical phenomena which were not

*) This does not mean that such bubbles could not change the overall flow in another way than by their displacement effect. In particular, for small gap width it is possible that the transition zone between the bubble and the external flow would have an effect on the profile behind it because of the reduced energy and the changed turbulence in the boundary layer and in this way, the separation in the overall flow would be changed.

included in the calculation, such as bubble effects and wake-boundary layer confluence.

Finally, the calculation was made with consideration of compressibility (dashed curve) that is for $Ma_\infty = 0.19$. This is approximately the (lower) critical Mach number at the lift maximum for $Re = 1.5 \cdot 10^7$. Because of the influence of compressibility, the lift maximum is displaced towards smaller angles of attack and is substantially reduced.

For these calculations, it was always assumed that the laminar turbulence transition occurs at the laminar separation point. 60 target points were used for the flap and 100 target points were used for the main wing. The computation time on the IBM 370/158 was 15-20 minutes for a set of parameters (α, Re, Ma_∞). /44

4. SUMMARY AND OUTLOOK

In numerical calculation method [6] for steady incompressible flow over profile systems with simple trailing edge,separation was extended to cases where there are several separation regions over the various parts of the profile system. It is only by describing this multiple separation that it becomes possible to calculate the lift curve in the vicinity of the maximum lift and in the post-stall range for mechanical high lift systems.

In the extended calculation method, in addition to multiple trailing edge separation, the influences of bubbles and compressibility were included for subsonic flows, approximately. The expanded method was programmed in FORTRAN and was tested with various examples. In all investigations, plausible unique solutions resulted. Comparison between theoretical results in measurements showed for the most part satisfactory agreement.

It was also found that the calculation possibilities are subject to some important restrictions:

a) steady plane flow is assumed. Unsteady effects for wing oscillations, gusts, acceleration, pulsating separation regions, etc., as well as three-dimensional effects over wings with finite stand are not covered.

b) It is assumed that the wakes of upstream wing parts (wake-boundary layer confluence) do not substantially influence the boundary layer directly. In practice, such influences often exist for moderate Reynolds numbers and small gap width.

c) Compressibility influences are only considered for pure subsonic flow and only approximately. In practice, local supersonic regions could certainly occur for high lift configurations. /45

d) Separation bubbles are only considered incompletely. On the profile topside, only short bubbles are allowed and these are only allowed to a limited extent and only as regarding their effects on the trailing edge separation. The empirical criteria present for the occurrence and bursting of such bubbles are incomplete and not very reliable.

Bubbles along the profile bottomside can only be roughly covered by estimated contour modifications with respect to their displacement effect. In practice, separation bubbles of all kinds occur, especially for not very large Reynolds numbers, and can substantially influence the overall flow under some conditions.

e) Our potential theory dead water model satisfies the condition of constant pressure only approximately (at three points) and according to experience, results in dead water pressure which is somewhat too high. For larger separation regions in this way, the moment and the drag are inaccurately calculated.

In addition, for separation over the main wing of a slotted flap configuration (section 3.1), a modeling which is too rough for the main wing wake could be the reason for unsatisfactory description of the flap flow.

f) The computer program can only be applied for trained persons in its present form because of continuous improvements. It is not yet optimized and it is insufficiently documented. It still does not contain the ground effect.

From all this, we have the following stimuli for future work:

- improvement, completion and documentation of the computer program
- development of a refined dead water model for strong and multiple separation
- better coverage of all bubble effects
- better coverage of compressibility influences, if possible for transonic flows
- consideration of wake, boundary layer confluence
- development of methods for three-dimensional and unsteady flows with separation

This further development cannot occur purely theoretically and will require substantial support of experimental work.

5. REFERENCES

[1] Riegels, F. W., Jacob, K. Calculation of pressure distribution of finite thickness profiles without and with flap and slats. ZFW 11 (1963) vol. 9, p. 357-367.

[2] Callaghan, J. G., Beatty, T. D. A theoretical method for analysis and design of multi-element airfoils. Journal of Aircraft Vol. 9 (1972) no. 12, p. 844-848.

[3] Mavriplis, F. Aerodynamic prediction and design methods of aircraft high lift systems. CANADAIR Rep. No. RAZ-000-381 (1973).

[4] Jacob, K. Calculation of the separated and incompressible flow over wing profiles and determination of maximum lift. ZFW 17 (1969) vol. 7, p. 221-230.

[5] Bhateley, I. C. A simplified mathematical model for the analysis of multi-element airfoils near stall. AGARD-CP 102, Lisbon, April 1972.

[6] Jacob, K., Steinbach, D. A method for prediction of lift for multi-element airfoil systems with separation. See also [6a] K. Jacob, DFVLR-AVA, IB 065-72A34 (1972). [6b] D. Steinbach, ZFW 2 1978, vol. 5, p. 293-305.

[7] Hayashi, M., Endo., E. Performance calculation for multi-element airfoil sections with separation. Trans. Jap. Soc. f. Aeron. a. Space Sciences Vol. 20 (1977), No. 49, p. 151-164.

[8] Olson, L. E. Optimization of multi-element airfoils for maximum lift. NASA Conf. Publication 2045, March 1978.

[9] Martensen, E., Sengbusch, v., K. Edge components of plane harmonic vector fields. Arch. f. Rat. Mech. a Analysis. Vol. 5 (1980), V. 1, p. 46-75.

[10] Jacob, K. Further development of a method for calculating the separated profile flow with special consideration of profile drag. DLR-FB 76-36 (1976).

[11] Rotta, J. C. FORTRAN-IV Calculation program for boundary layers for compressible plane flows and axisymmetric flows, DLR-FB 71-51 (1971).

[12] Jacob, K., Neher, M. Program for calculating profile coordinates. DFVLR-AVA IB 230-73 R 03 (1973).

[13] Jacob, K. Calculation of incompressible flow around thick wings and cascade profiles with corner trailing edge. ZFW 15 (1967) V. 8/9, p. 341-346.

[14] Jacob, K. The influence of separation bubbles on the lift of wing profile. DLR-FB 77-34 (1977), p. 111-123.

[15] Jacob, K. The influence of compressibility on the lift of wing profiles for subsonic flow with separation. DFVLR-IB 251-78 A 06 (1978).

[16] Wentz, W. H., Seetheram, H. C. Development of a Fowler flap system for a high performance general aviation airfoil. NASA CR-2443 (1974).

[17] Wentz, W. H., Seetheram, H. C., Fiscko, K. A. Force and pressure tests of the GA(W)-1 airfoil with a 20% aileron and pressure tests with a 30% flap. NASA CR-2833 (1977).

[18] Abbott, I. H., Doenhoff, v., A. F., Stivers, L. S. Summary of airfoil data. NACA Report no. 824 (1945).

[19] Dvorak, F. A., Maskew, B. The prediction of $c_{l\,max}$ using a separated flow model. Journ. of the Amer. Helicopter Soc. Vol. 23 (1978), no. 2, pp. 2-8.

[20] Baumert, W., Enghardt, K. The component measurements for a rectangular wing with flap and downward pointed nose. DFVLR-AVA IB 71 C 29 (1971).

Figure 1.

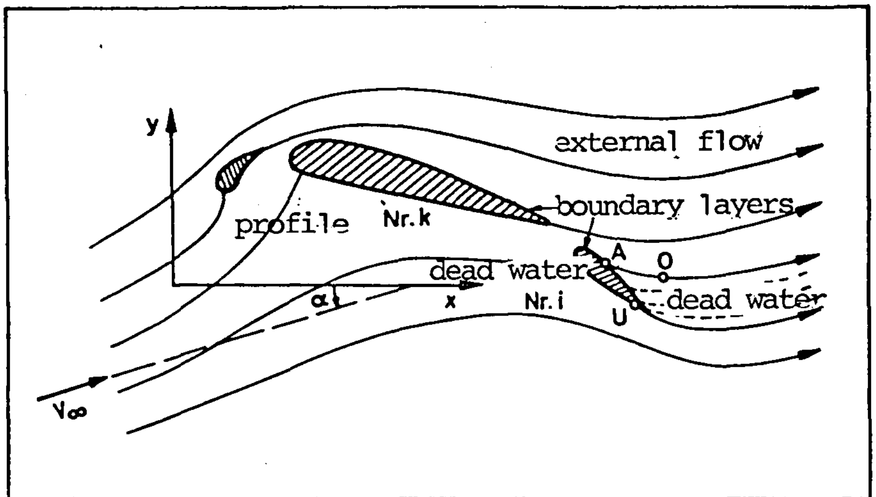

Flow around the profile system with simple trailing edge separation

Figure 2.

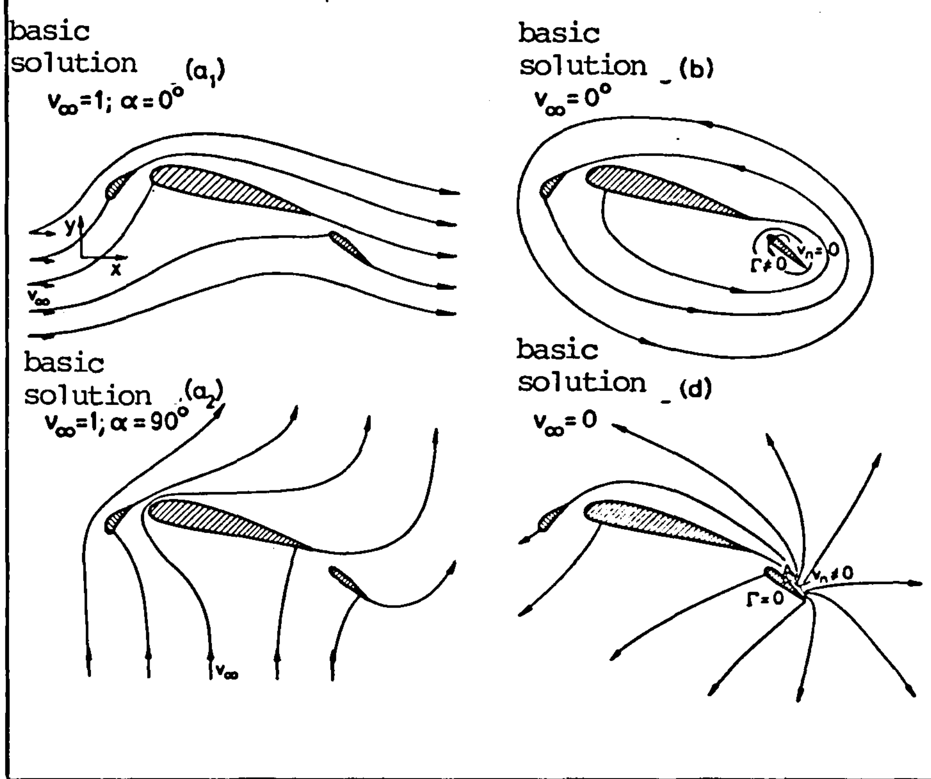

Flows of the basic solutions

Figure 3.

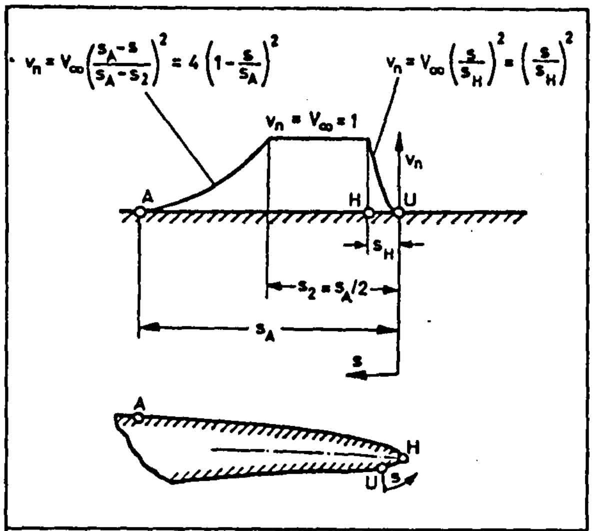

Standard source occupation

Figure 4.

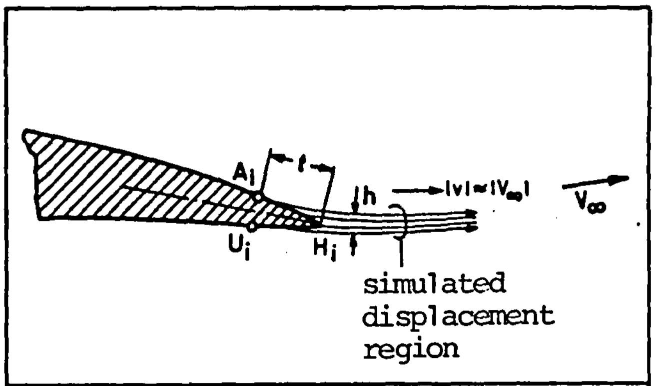

Simulated displacement effect for reduced separation

Figure 5.

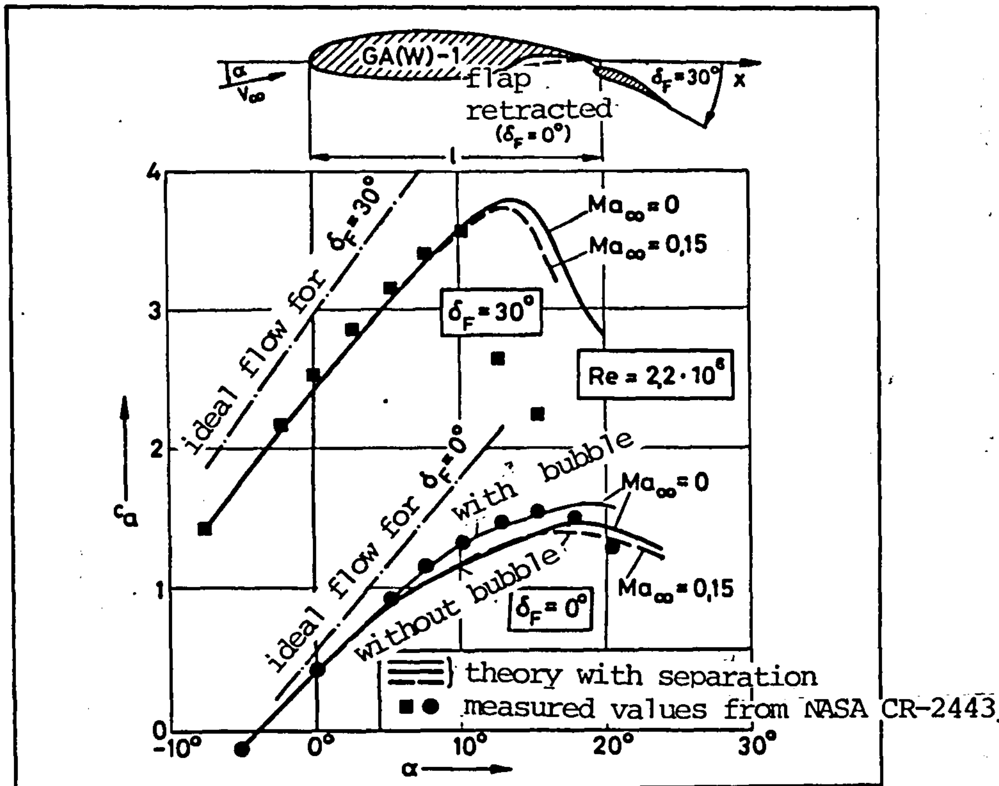

lift curves for profile with and without Fowler flap

Figure 6.

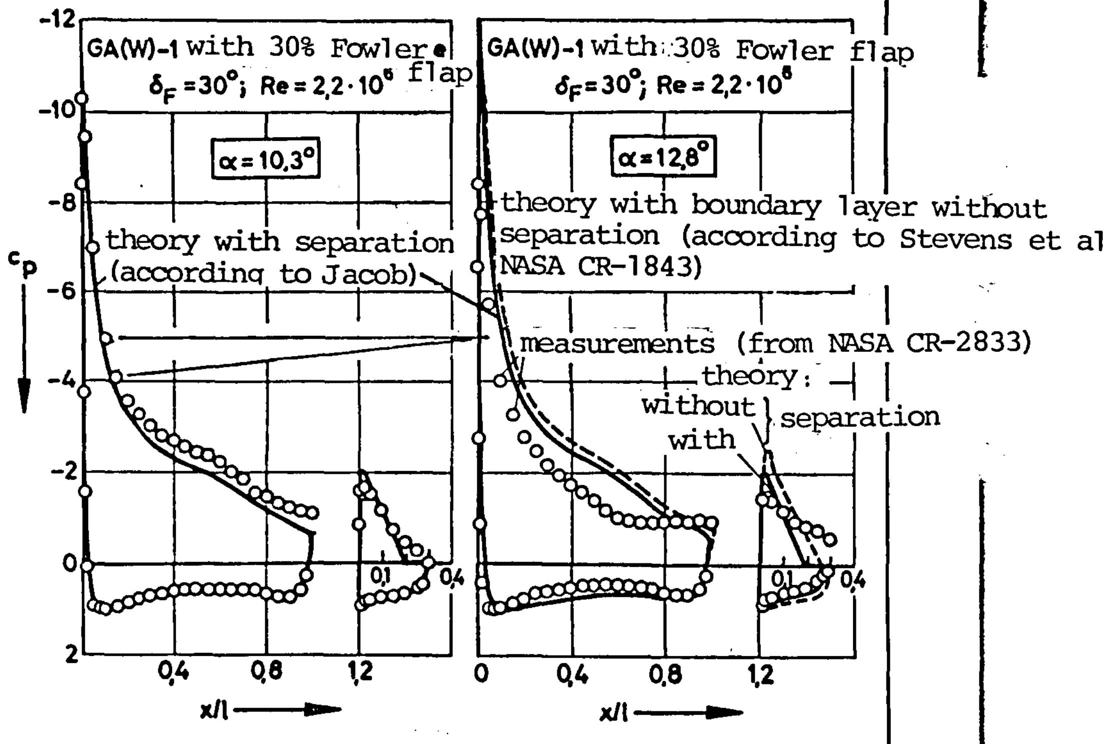

Pressure distribution for profile with Fowler flap for two different angles of attack

Figure 7.

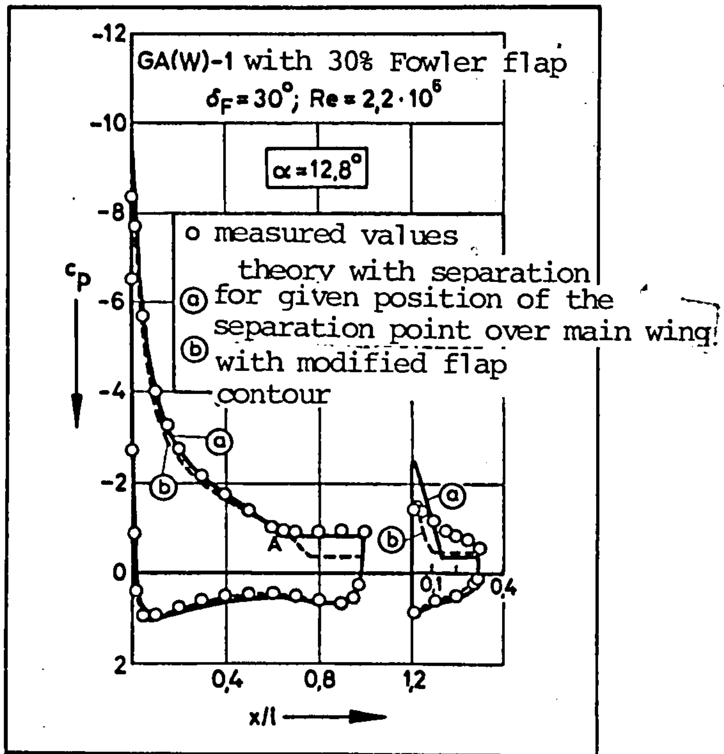

Pressure distributions for profile with Fowler flap with different boundary conditions

Figure 8.

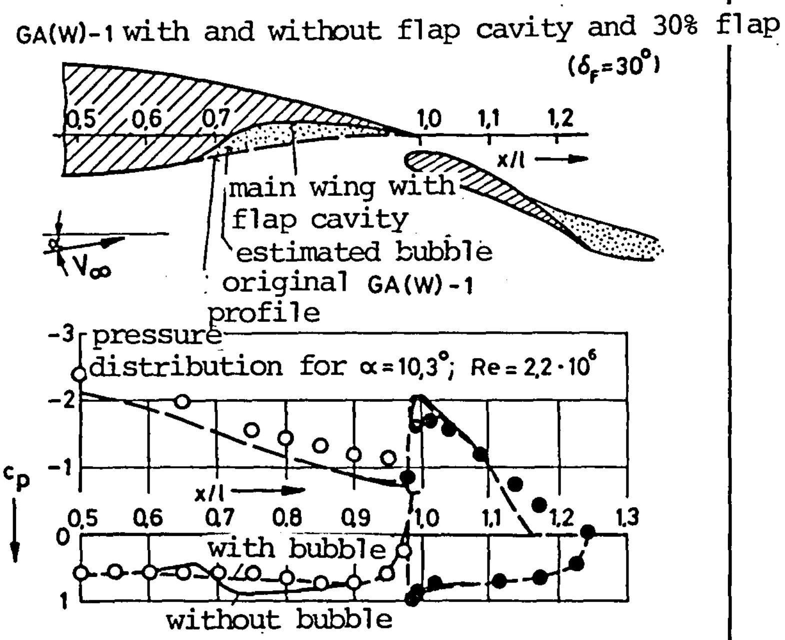

Pressure distribution for profile with Fowler flap with and without bubble in the flap cavity

Figure 9.

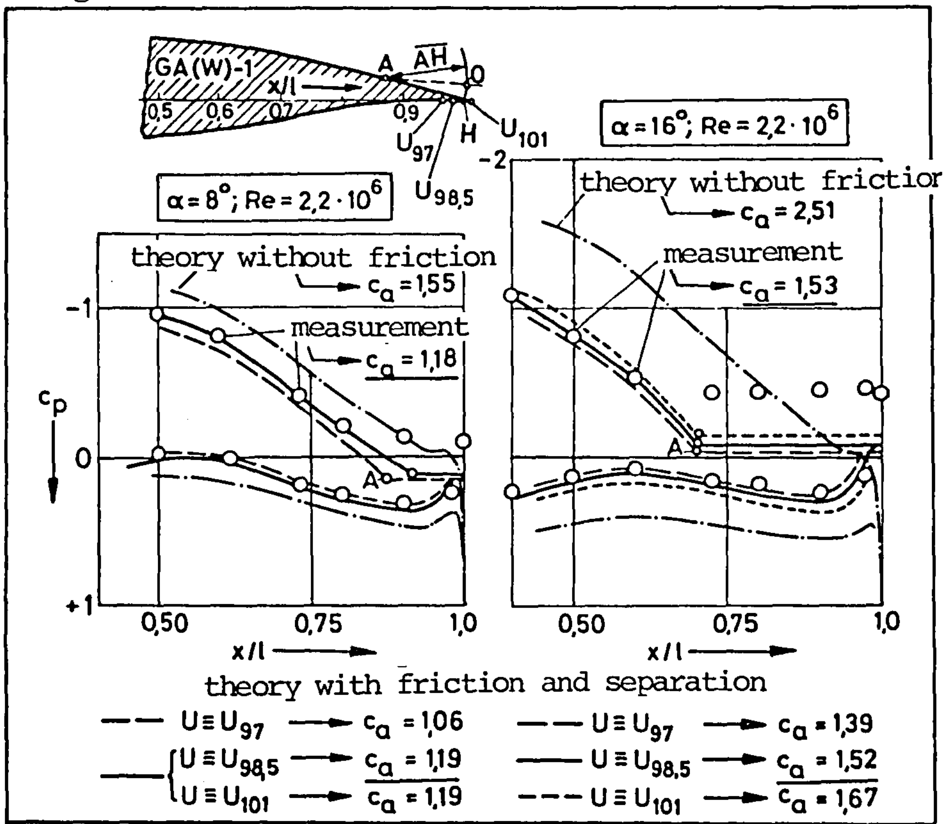

Pressure distributions for single profile for different positions of comparison point U

Figure 10.

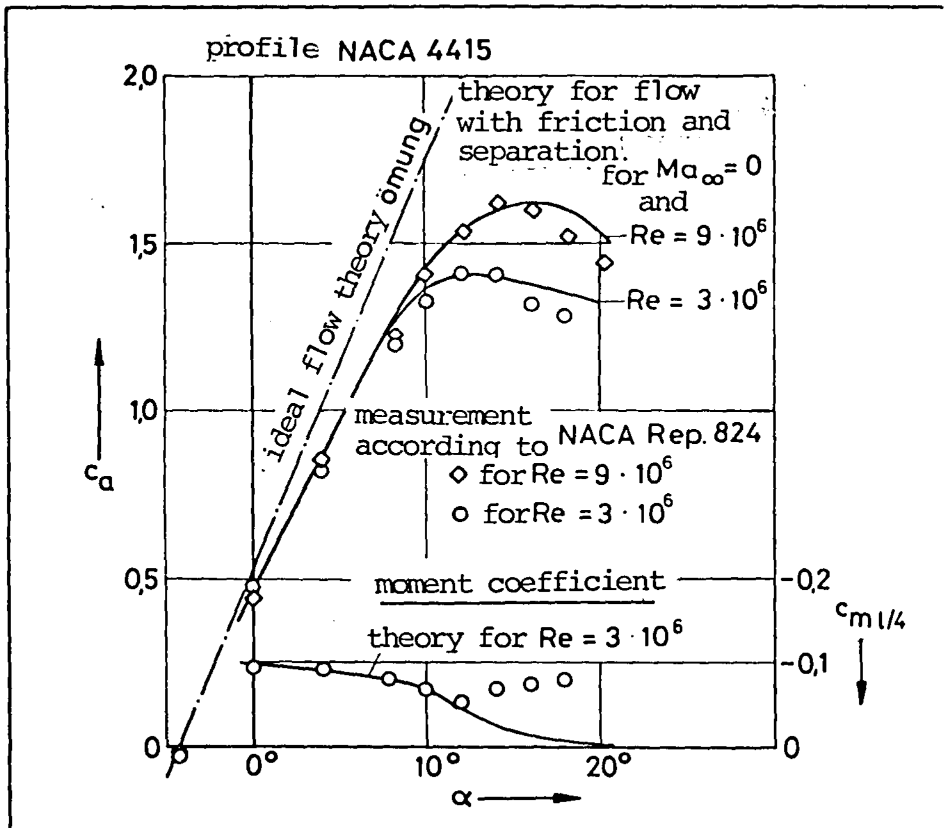

Lift and moment for a single profile.

Figure 11.

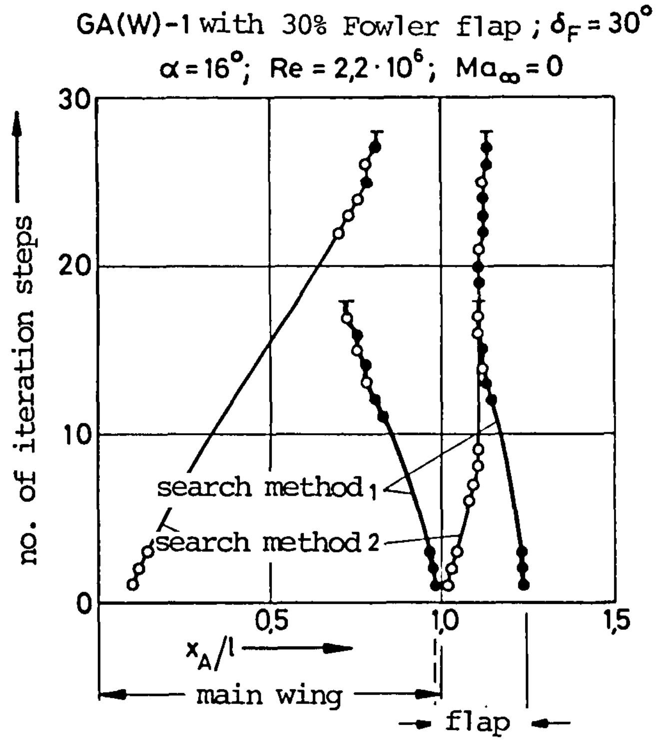

● attachment points, ahead of which there was separation
o attachment points, ahead of which there was no separation

Iteration in the search for separation points for profile with Fowler flap

Figure 12.

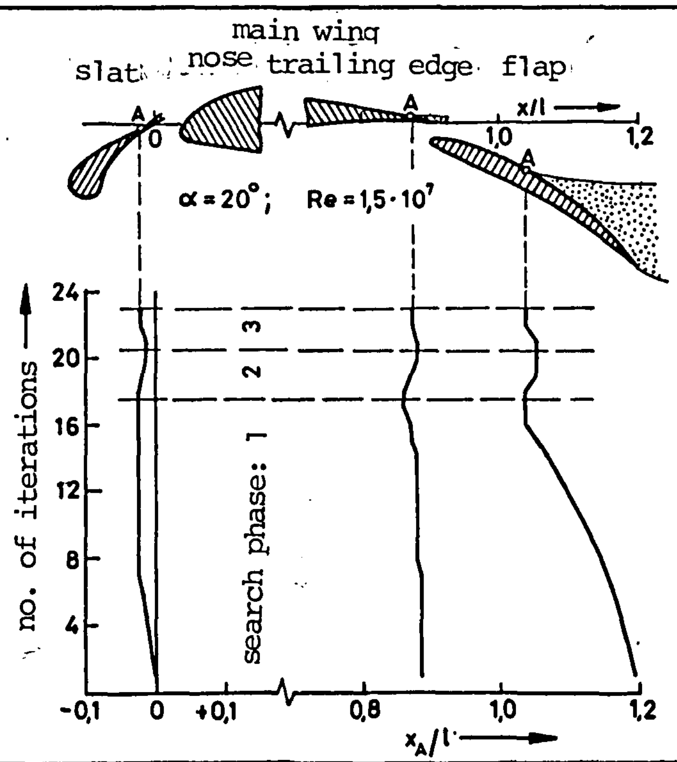

Iteration for the combined search method for a three-part profile system

Figure 13.

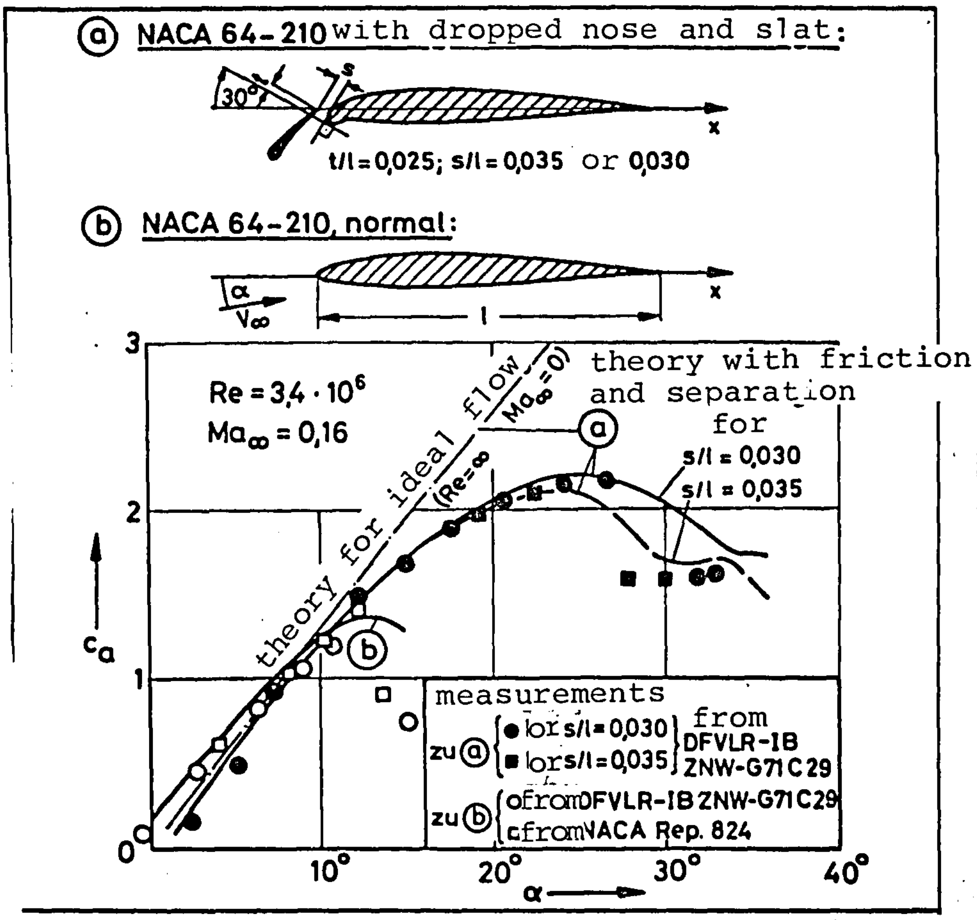

Lift curve for a profile without and with slat for various gap size.

Figure 14.

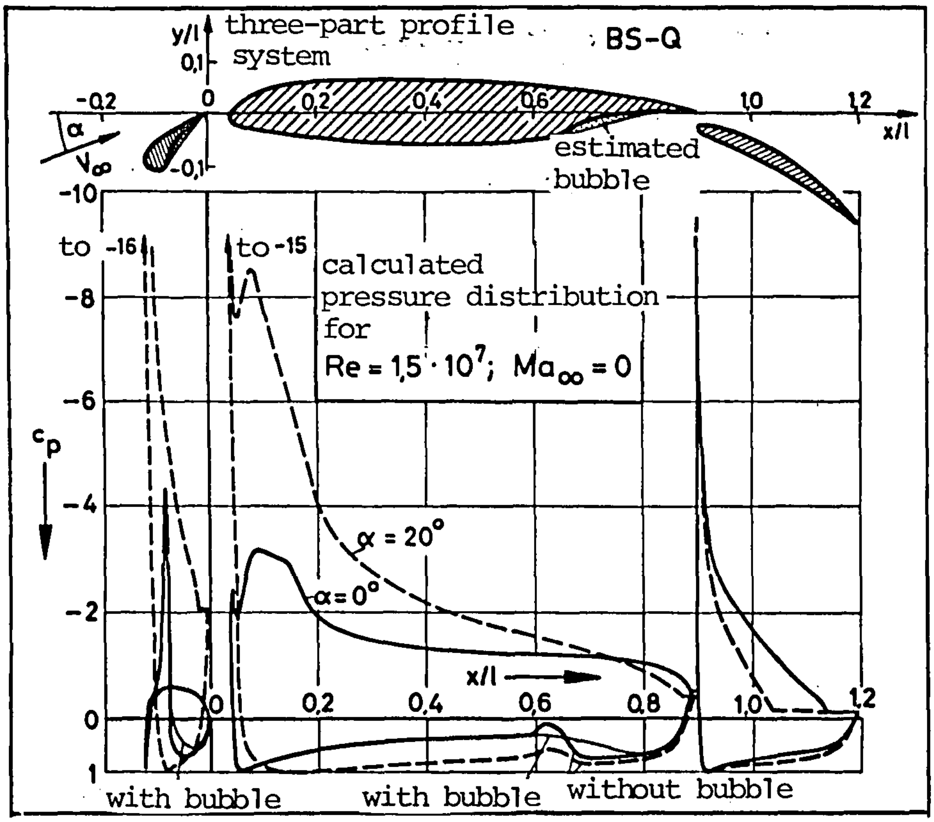

Pressure distributions for a Three Part high lift system, for two different angles of attack.

Figure 15.

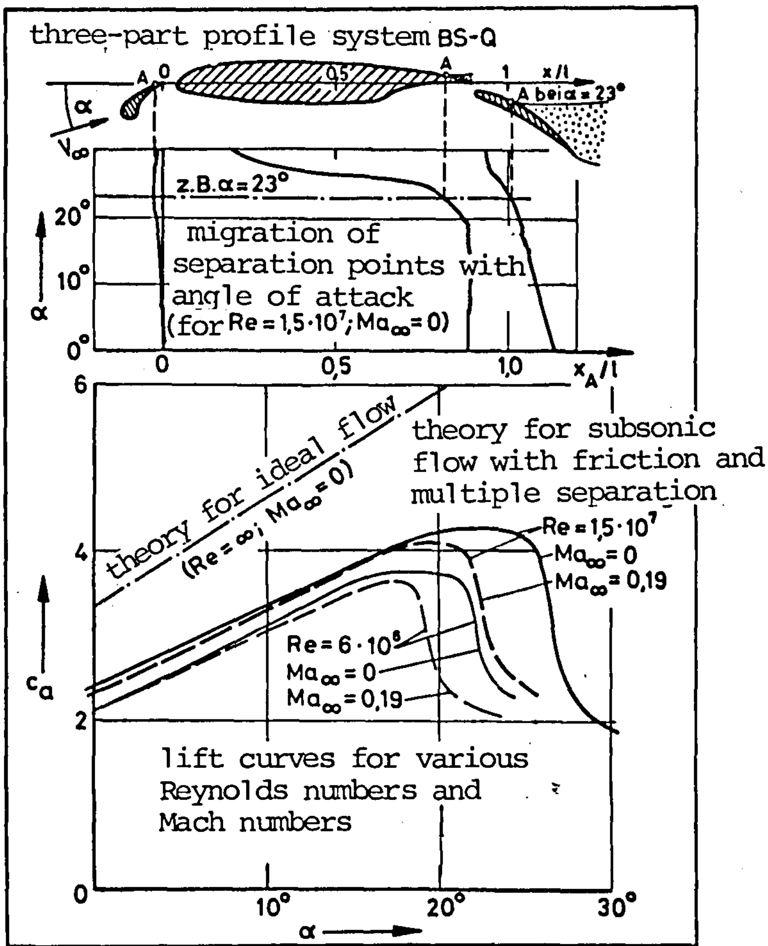

Increase of separation and lift curves for a three part high lift system.

End of Document